LEOSPHERE Pulsed Lidar Principles

Contribution to UpWind WP6 on Remote Sensing Devices

Jean-Pierre Cariou & Matthieu Boquet - LEOSPHERE, Orsay, FR

Abstract

This report complements the description of the measurement process for a Doppler lidar for wind speed and direction determination, by focusing more on the pulsed lidar technology, and particularly on the WINDCUBE™ Doppler pulsed lidar, one of the most accurate remote sensing devices available at the present time in the wind industry.

Content

Table of figures

1. Introduction

There is a pressing need for good wind-speed measurements at greater heights and at more site locations to assess the availability of the resource in terms of power production and to identify any frequently occurring atmospheric structural characteristics that may impact the operational reliability and lifetime of wind turbines and their components. To measure the wind field up to the height of new generation wind turbines and at any location of interest, remote sensors are needed to complement masts.

Different technologies are in use in this field, among them pulsed lidars (LIght Detection And Ranging). The underlying principle of pulsed lidar measurement of wind and aerosols is the use of optical heterodyne (coherent) detection, in which laser pulses are transmitted into the atmosphere and scattered off of naturally-occurring small dust particles (aerosols) entrained in the ambient flow field ([8], [10], [11] and [12]). Even though the measurement principle is well known and similar to pulsed radars, pulsed lidars have only been used in wind energy site assessment only for 4 years. Their recent introduction is mainly due to laser revolution coming from fiber telecommunication development in the late 90s.

In this chapter, we describe the architecture of pulsed lidars, based on the WINDCUBE™ lidar developed by LEOSPHERE and ONERA, the French Aerospace Lab. We define the different modules of a pulsed lidar, their specific functions and the individual level of uncertainties they might bring to the lidar wind speed retrieval. We also show the differences between pulsed and continuous wave lidars, used as well for wind sensing. We eventually give the lidar equation in pulsed mode, giving the relationship between parameters, and we focus on range and speed accuracy and resolution.

2. End-to-end description of pulsed lidar measurement process

2.1. Architecture of pulsed lidars

Figure 1 illustrates the general set up of a pulsed lidar. The following paragraphs provide more details of the key hardware components and explain the requirements and trade-offs on solutions for the main parts of the lidar.

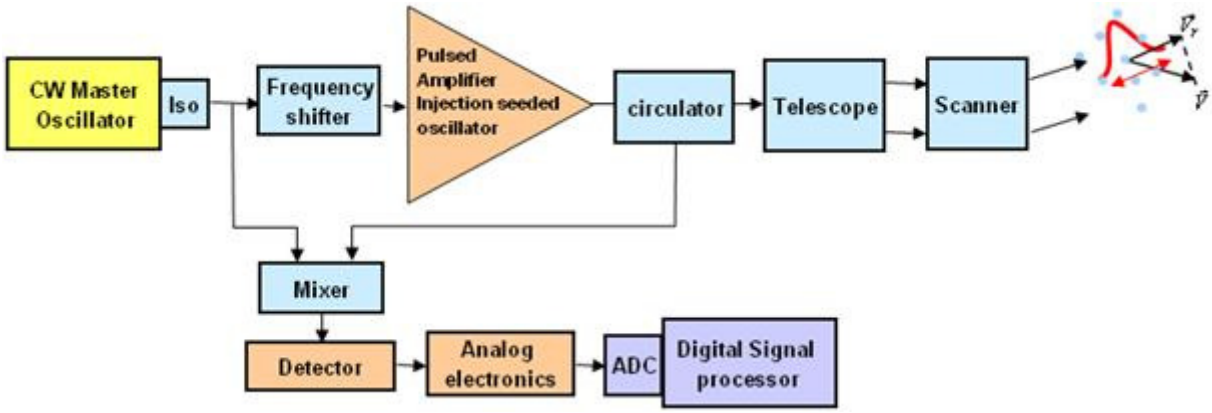

Figure 1 Pulsed Lidar set up

2.1.1. Laser source

A pulsed lidar needs a continuous wave laser, called Master Oscillator (MO) to generate the Local Oscillator (LO) beam and a pulsed laser to generate the powerful transmitted pulse. The frequency offset between the two sources need to be stable with time to allow an unbiased measurement of the Doppler shift.

The master oscillator provides the laser wavelength, the laser linewidth, the laser intensity noise and the state of polarization. Each of these parameters has to be well known and stable to guarantee the lidar performance. The CW power is at least some milliwatts.

The pulsed laser delivers cyclic pulses of high energy. The pulse duration τ is some hundreds of nanoseconds, that determines the length of the pulse in the atmosphere and so the spatial resolution.

The Pulse Repetition Frequency (PRF) is as high as possible, but cannot exceed a maximum value PRF_{max}. To avoid ambiguity between return signals, the time between pulses (1/PRF) must be longer than the round trip time of flight of the pulse to the greatest height to be measured.

$$PRF_{max} = \frac{C}{2Z_{max}}$$

Pulse duration (ns)	Pulse length (m)	Minimum spatial resolution (m)
200	60	30
400	120	60
800	240	120

Table 1 Spatial resolution versus pulse duration

PRF(KHz)	Max range (m)
10	15000
20	7500
50	3000

Table 2 PRFmax versus lidar range

Two technologies are used for the pulsed laser. In the first one, called MOPA (Master Oscillator Power Amplifier), pulses are emitted from the MO by use of an optical shutter. Resulting low power pulses are amplified into a single pass high bandwidth optical amplifier to generate high power pulses, having the same duration, frequency and polarization as the incoming pulses. In the second scheme, the MO is used as a seeder in a Q-Switch pulsed laser. Cavity frequencies have to be matched to allow the seed frequency to be amplified. Pulse duration and PRF depend on the cavity parameters. First solution allows higher PRF but lower energy/pulse than the second one. Both deliver an equivalent average power.

Laser wavelength is an important parameter. Following the recent improvement of solid state lasers in late 90s, the near Infrared spectrum (1.4µm - 2.2µm) is widely used for operational wind lidars. Efficient technology, good Doppler sensitivity, fiber architecture, eye safety and good atmospheric transmission are the main reasons ([13]).

2.1.2. Circulator

Figure 2 describes the circulator and the different elements which compose it. The function of the circulator is to transmit the laser pulse from the laser (1) to the telescope (2) and to direct the backscattered light from the telescope (2) to the receiver (3). Power handling, transmission efficiency and isolation between (1) and (3) ports are critical parameters. In coherent pulsed lidars, most circulators use polarization to perform this function. Polarization is rotated in the telescope thanks to a quarter wave plate. The transmitted polarization is circular.

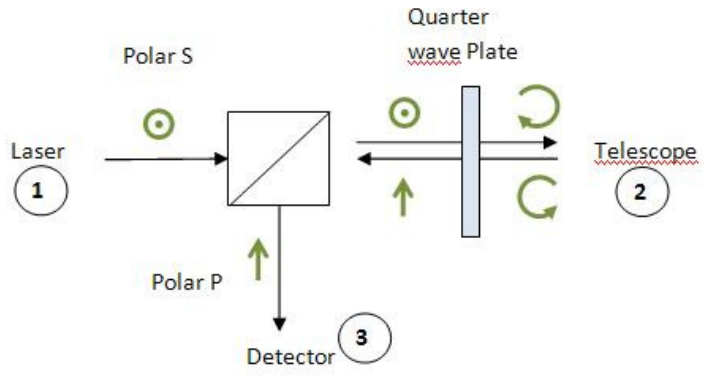

Figure 2 Circulator

2.1.3. Telescope

The telescope magnifies the laser beam in order to reduce its divergence in the far field, and focuses the beam at any distance. The larger the beam, the smaller the divergence and the better the SNR at long range. Since the lidar signal/noise ratio is inversely proportional to the beam area, beam diameter must be minimized on the global measurement range to ensure maximum efficiency.

The telescope can use reflective or refractive optics, perfectly corrected from geometrical aberrations. In order to lose less than 3dB on the detection efficiency, wavefront distortion on the global optical path has to be less than λ/4 RMS, including components and atmospheric distortion.

Atmospheric turbulence creates wave distortion that degrades heterodyne efficiency. To keep this distortion negligible, the telescope aperture has to be smaller than the coherence diameter of the beam expressed by:

$$d_0 = 2.4\ 10^{-8} \lambda^{6/5} Z^{-3/5} Cn^{-6/5}$$

Considering nominal values of index structure constant ($Cn^2=10^{-14}$ $m^{-2/3}$) and propagation over about Z=1km, this limits the size of the telescope to about 10cm at ground level.

2.1.4. Scanner

Coherent lidar measure the radial component of the wind, i.e. the projection of the wind vector on the Line of Sight (LOS). To provide two or three components of the vector, the beam has to be directed in two or three independent different directions (more details in 2.7. Wind vector reconstruction). The scanner can move the entire telescope (for example Mitsubishi [15]) or only the beam. Some manufacturers prefer skipping the scanner and duplicate the telescope to suppress all moving parts from the lidar (for example Catch The Wind).

To perform the vertical wind profile, beams are directed upwards along a cone around the zenithal direction. For that, a single rotating prism or dual flat mirrors are used (see Figure 3).

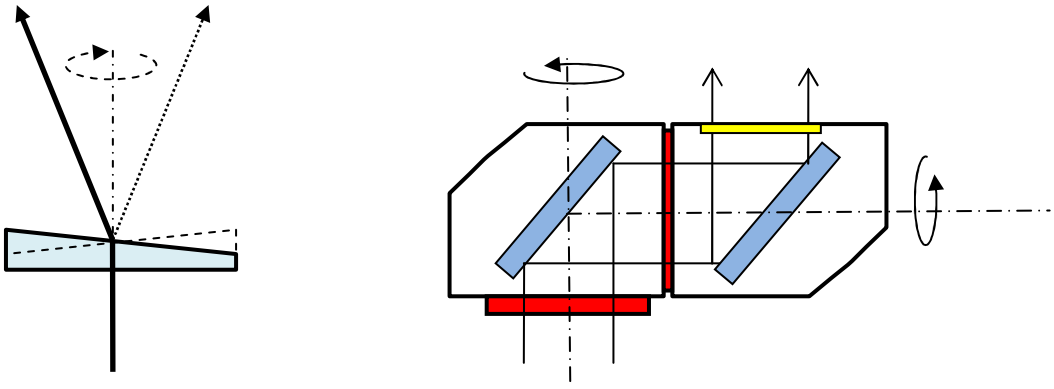

Figure 3 Prism scanner and dual flat mirror scanner

To measure the wind speed in any direction, and display 2D or 3D wind maps, a more flexible scanner is needed. Double flat mirror scanners are mostly used (CTI, Halophotonics, Leosphere), while double prism scanners (Risø DTU Windscanners [16]) offer a more original and compact solution. A global hemispherical field of view can be obtained with both solutions.

2.2. Differences Pulsed vs. Continuous Wave lidars

In CW lidars, light is continuously transmitted to the atmosphere. Assuming atmospheric parameters do not vary, the backscattered signal average power is constant, coming from all distances at the same time. The distance weighting function is defined by the beam aperture and the focus distance (see "Remote Sensing QinetiQ Lidar Measurement Report"). Spectral bandwidth is limited by atmospheric turbulence if laser line width is narrow. The size of the range gate (contributing to the signal) increases as the square of the distance. The range gate can be small and well defined in short distance but is always too large when the range exceeds few hundreds of meters

In pulsed lidars, short pulses are sent to the atmosphere, illuminating at each instant only a limited part of the line of sight. Therefore, backscattered signal arriving onto the detector at a time only comes from a given range of distance. The time delay between the pulse start and the measurement time informs on the distance of the analyzed zone. The range gate length is always the same, at short and long range.

Pulsed LIDARs, as their name implies, emit regularly spaced emissions of highly collimated light energy for a specified period of time (pulse length). Precision timing circuits then isolate the returned signals to a period of time that corresponds to a specified segment of radial distance along the beam called a range gate. The backscattered signals contained within each gate are then processed to derive the radial velocities along the path of the LIDAR beam.

Next table summarizes the main differences between CW and pulsed lidars:

	CW lidar	Pulsed lidar
Velocity accuracy	limited by coherence time of the atmosphere	limited by the pulse duration
Range gate	determined by focus increases as R^2	constant, around $c\tau/2$
Number of range gates	Less than 10, sequentially addressed	More than 100, simultaneously addressed limited by SNR at long range
Sensitivity to targets out of focus	high	no
Max range	Few hundreds of meters	some kilometers
Laser source	1 laser	Master Oscillator + Power Amplifier
Laser technology	large average power	limited average power
Polarization	not necessary	mandatory

Table 3 Main differences between CW and pulsed lidars

2.3. Signal processing

After the pulse has left by the laser, the detector starts to collect the backscattered signal from the successive range gates. It first crosses the telescope optics and provides a zero Doppler signal, used as a marker for the zero distance. Even if the stray light is small thanks to optimized coatings (10^{-6} order), this signal is always larger than the light backscattered by the atmosphere (10^{-12} order).

Each layer of atmosphere then backscatters light to the lidar. The power is proportional to the backscattering atmospheric coefficient β while the frequency shift is proportional to the radial velocity. For each pulse, the collected signal contains the total wind speed information on the LOS.

However, both the signal and the noise fluctuate from pulse to pulse and it is necessary to average signals to get a good estimation of the spectral content. Because of the short wavelength (10^4 less than radars and sodars), signal phase changes quickly with particle motion, atmospheric turbulence and small laser spectral drifts. This is useless to average time series. To improve SNR on the Doppler spectrum, successive spectra corresponding to the same range gate are summed. SNR increases as the square root of the number of averaged pulses N. This computation is performed for all range gates.

To sum up, the successive steps for the signal processing are for every LOS (Figure 4):

- Break the time series into gates
- Compute the spectrum for each gate
- Average spectra for same range gate from different pulses
- Find frequency peak for each gate to find Doppler shift and convert to radial velocity
- Reconstruct wind vector for each gate with radial velocity on the different LOS.

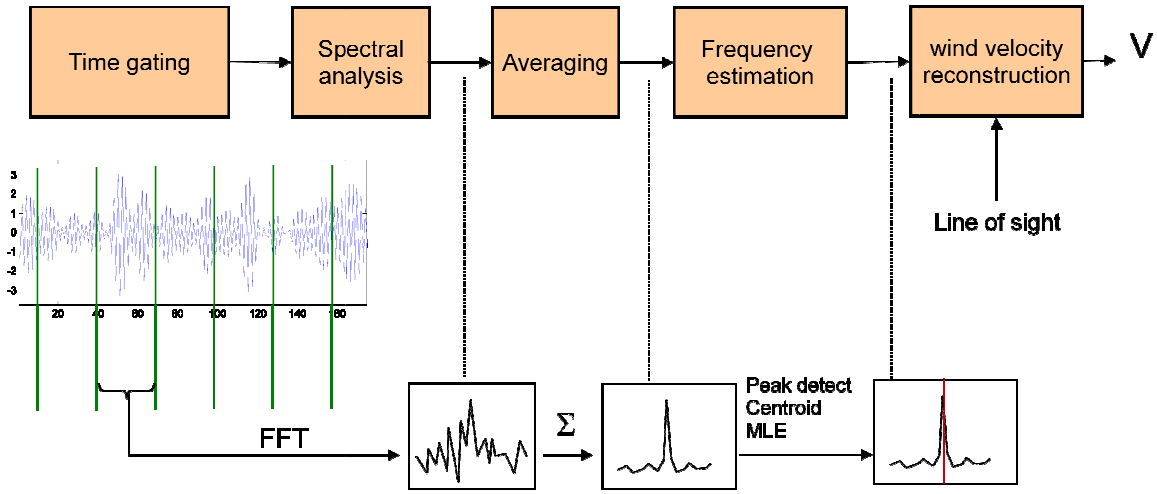

Figure 4 Radial wind velocity retrieval process

2.4. Coherent detection

Basic principles of coherent detection are the same than for CW lidars (see "Remote Sensing QinetiQ Lidar Measurement Report"). The return signal mixes with local-oscillator creating the beat signal. The electronic signal on the detector contains the same amplitude, frequency and phase information as the optical signal, but is frequency downshifted to allow detection with conventional high speed detectors. So the Doppler shift, which is small in comparison to the optical frequency ν can be measured in base band. To allow both negative and positive shifts to be measured, an offset frequency F_i (Intermediate frequency) is added on one arm of the interferometer.

$$F_{dop} = (\nu + F_i) - \left(\nu + F_{dop}\right) = F_i + F_{dop}$$

$$LO \qquad signal$$

An important advantage of coherent detection is that it can be limited by signal photon noise, if some conditions are fulfilled. First condition is that the amplitude and phase match between signal beam and the LO beam must be perfect. The second condition is that temporal coherence is optimum, i.e. the spectral width of the main oscillator must be narrower than the spectral width of the electronic signal. The third condition is that polarization state must be the same on the LO and the signal. System and component limitations lead however to a loss in heterodyne efficiency. Kavaya and Frehlich ([3]) demonstrated that the heterodyne efficiency is limited to 40% by spatial coherence for a perfect Doppler lidar using a circular aperture and a Gaussian beam. A good actual operational lidar heterodyne efficiency is more than 20%.

2.5. Lidar Equation

The lidar equation gives the expected signal power coming back from the atmosphere within the range gate to be analyzed. The signal power can then be compared to the noise power in order to determine the range of the lidar.

The total optical power $P_r(Z)$ reflected back in the receiver telescope from the range gate at Z is:

$$\mathrm{P_r}(Z) = P_{peak}.T_{inst}.T_{atm}.\beta_\pi(Z).\frac{c\tau}{2}.\Omega$$

Where:

- P_{peak} (W) is the transmitted pulse peak power
- T_{inst} is the instrumental round trip transmission
- T_{atm} is the atmospheric round trip transmission:

$$T_{atm} = \exp\left(-2\int_0^Z \alpha(x)dx\right)$$

- $T_{atm} = \exp(-2\alpha Z)$ if atmosphere is homogeneous
- $\beta_\pi(Z)$ ($m^{-1}sr^{-1}$) is the backscattering coefficient of the atmosphere at distance Z
- τ is the FWHM pulse duration (Full Width Half Maximum)
- Ω is the reception solid angle:

$$\Omega = \frac{\pi\sigma^2}{Z^2}$$

- σ is the efficient telescope aperture radius. α and β_π are roughly proportional since they both depend on aerosol concentration in the atmosphere.

However, because of limited heterodyne efficiency, only a part of $P_r(Z)$ is efficient for the coherent detection. The inefficient part of $P_r(Z)$ comes from phase and polarization mismatches.

An interesting way to estimate the antenna lobe of the detection is to propagate back in the atmosphere the LO, and to compute the overlap integral of the signal and LO along the LOS. This defines the transverse and longitudinal efficiency of the lidar (BPLO theory [2]).

The efficient signal power incoming onto the detector is:

$$P_s(Z) = P_{peak}.T_{inst}.T_{atm}.\beta_\pi(Z).\frac{c\tau}{2}.\lambda.\mathrm{I(Z)}$$

I(Z) is a Lorentzian function including Ω and Z depending focus function.

$$I(Z) = \frac{\Delta Z}{(Z - Z_0)^2 + \Delta Z^2}$$

- With: $Z_0 = \frac{F_t}{1+\left(\frac{F_t}{Z_r}\right)^2}$; $Z_r = \frac{\pi}{\lambda}.\sigma^2$; $\Delta Z = \frac{Z_0 F_t}{Z_r}$

- Z_0: distance where I(Z) is maximum, i.e. signal to noise is maximum
- Z_r: Rayleigh distance
- F_t: instrumental geometrical focus distance (wave curvature radius at telescope)
- ΔZ : half of FWHM geometric depth of focus

Figure 5 shows different plots of the Lorentzian function I(Z) for different values of the focus distance Ft. Short focus improves signal power at short range whereas long focus averages the power along the distance, leading to a more constant signal on the different range gates, but with a lower value.

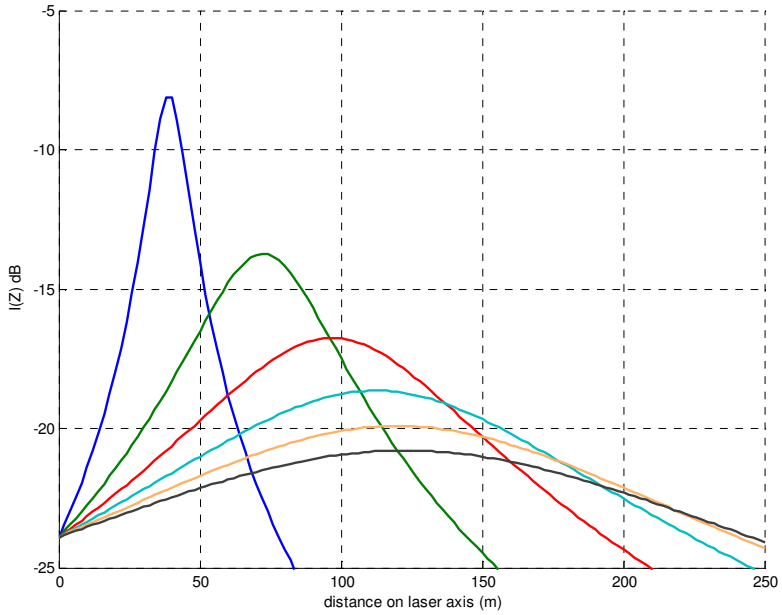

Figure 5 Variations of Lorentzian function I(Z) with focus distance Ft = 40, 80, 120, 160, 200, 240m respectively.

Figure 6 shows different plots of the Lorentzian function I(Z) for different values of the telescope aperture radius σ. The focus distance Ft is changed so that Z_0 is constant. It is shown that large σ give higher received power at Z_0 but lower power far from Z_0. So, if the range of interest is large, it is better to optimize σ so that received power is as constant as possible in the range.

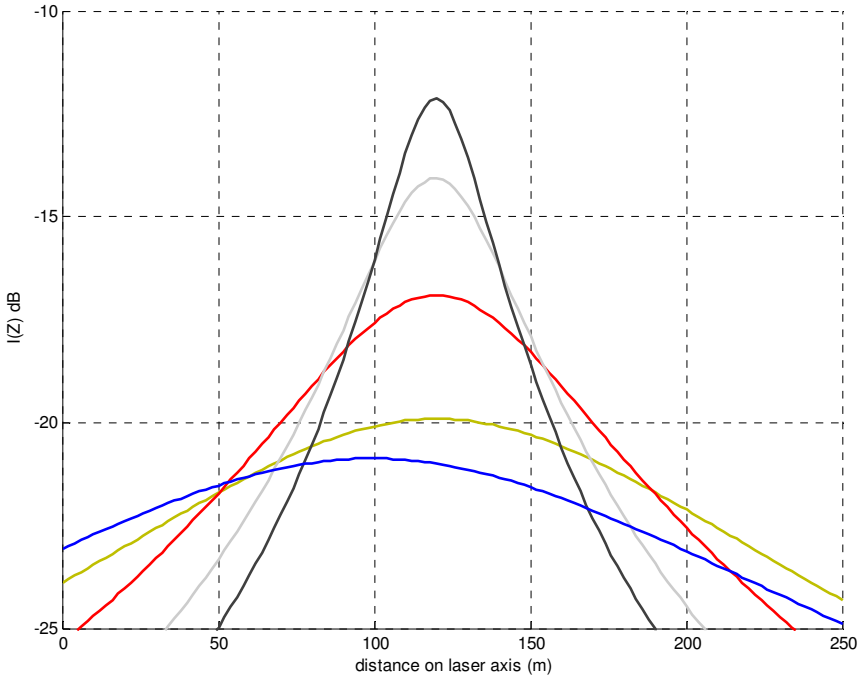

Figure 6 Variations of Lorentzian function I(Z) with aperture radius σ = 10, 11, 13, 17, 21mm respectively

The current power on the detector can then be derived using the same equations as in CW mode.

$$\langle i^2{}_{het}\rangle = 2\eta_{het} S^2 P_{LO} P_s(Z)$$

With:

- P_{LO}: Local oscillator power (W)
- η_{het}: heterodyne efficiency (depends on phase, amplitude and polarization matching)
- S : detector sensitivity (A/W)

$$\eta_h = \frac{\left[\iint_{Ad} E_s(x,y).E_{lo}^*(x,y)dxdy\right]^2}{\iint_{Ad} E_s^2(x,y)dxdy.\iint_{Ad} E_{lo}^2(x,y)dxdy}$$

- $\langle i^2{}_{het}\rangle = \eta_{het} T_{inst}\, T_{atm}.S^2\, \beta_\pi(Z) P_{LO} P_{peak}$ τc I(Z)

The lidar equation shows that signal power is proportional to pulse energy $P_{peak}\tau$ and proportional to LO power. Local Oscillator amplifies the signal allowing it to be detected over the detector noise.

2.6. Spectral processing MLE

A maximum likelihood estimator based on the likelihood of the Fourier transform of the signal is used as spectral processing. This estimator assumes an uncorrelated Fourier transform in order to use data obtained from the accumulated spectrum. The estimator is slightly different from the likelihood of the spectrum traditionally used for spectral maximum likelihood estimators but still shows the same efficiency.

Signal spectrum is calculated using a temporal model such as the Feuilleté model ([9]) and thus takes into account all the FFT algorithm disturbing effects such as the spectral leakage, which must be carefully characterized in the case of a pulsed atmospheric lidar.

Since the lidar signals are statistically independents, the joint probability of the whole lidar signals can be defined as the product of the probability of each signal:

$$P_{\left(I_{s_1},\ldots,I_{s_M}\right)}\left(I_{s_1},\ldots,I_{s_M}\right) = \frac{1}{\left(\pi \det(R)\right)^M} e^{-\sum_{k=1}^{M} I'_{s_k} R^{-1} I_{s_k}}$$

With I_{sk} the FFT of the k_{th} lidar signal in the range gate analyzed and R is the covariant matrix of the FFT of the signal. This joint probability leads to the following expression of the likelihood:

$$\ln P_{(I_{s_1},\ldots,I_{s_M})}(I_{s_1},\ldots,I_{s_M}) = -MN\ln\pi - M\ln\left(\det(R)\right) - \sum_{k=1}^{M} I'_{s_k} R^{-1} I_{s_k}$$

The performances of the MLE tend asymptotically (for a number of accumulated spectrums as low as 10) to the Cramer-Rao Lower Bound (CRLB). The CRLB is given by the inverse of the Fisher information matrix, which can be expressed ([5]) as:

$$F_{kl} = trace\left(R^{-1}\frac{\partial R}{\partial \theta_k} R^{-1}\frac{\partial R}{\partial \theta_l}\right)$$

With θ_k is one of the 3 parameters to be estimated, such as the CNR, the mean wind speed or the wind speed dispersion within the range gate.

Under the assumption of an uncorrelated spectrum, the likelihood can be expressed as a function of the accumulated spectrum:

$$\ln(P) = MN\ln\pi - M\sum_{i=1}^{N}\ln\left(S_s\right)_i - \sum_{i=1}^{N}\sum_{k=1}^{M}\frac{(S_{s_k})_i}{(S_s)_i}$$

With $(S_{Sk})_i$ is the i_{th} sample of the spectrum of the k_{th} signal and $(S_S)_i$ is the i_{th} sample of the spectral model, and a function of the CNR, the mean wind speed and the wind speed dispersion.

Spectral approaches ([1], [4], [6]) assume an uncorrelated accumulated spectrum described by a gamma statistics of parameter M:

$$\ln(P) = N\ln\left(\frac{M^{M-1}}{\Gamma(M)}\right) + (M-1)\sum_{i=1}^{N}\ln\left(\frac{1}{M}\sum_{k=1}^{M}(S_{s_k})_i\right) - M\sum_{i=1}^{N}\ln\left(S_s\right)_i - \sum_{i=1}^{N}\sum_{k=1}^{M}\frac{(S_{s_k})_i}{(S_s)_i}$$

This likelihood based on the signal spectrum is more complex than the likelihood of the FFT and therefore the former is preferred.

2.7. Wind vector reconstruction

Pulsed lidars provide radial wind components on different lines of sight at different altitudes. In an ideal case, and to mimic local sensors such as cup or sonic anemometers, beams intersect at the point of interest within a small volume. This is the goal of the Windscanner.dk ([16]) project with three lidars. In an operational situation, only one lidar is available. To reconstruct the 3D components of the wind vector, some assumptions are then necessary.

- Horizontal homogeneity: the three components of the wind are the same for the different points of the disc at a given altitude. The numerous measurement campaigns have proven that this assumption is valid on flat terrains and offshore, but not perfect on complex terrains (hills, mountains, forest boarders)
- Temporal variations are slower than the inter-beam distance divided by the horizontal wind speed. This time increases with altitude and matches the conical geometry.
- Wind slowly varies within a range gate. Wind dispersion lowers the SNR and provides a bias if the shear is non linear.

The scanning configuration can be either Velocity Azimuth Display (VAD) or Doppler Beam Swinging (DBS). VAD uses information from a continuous scan in a part or total cone angle and is mostly used in CW lidars. DBS is used in pulsed lidars to average more information on the LOS. Since VAD is described in the “Remote Sensing QinetiQ Lidar Measurement Report”, we focus here on DBS reconstruction.

First is important to define an orthogonal frame. The orthogonal frame of the WINDCUBE™ is described in Figure 7:

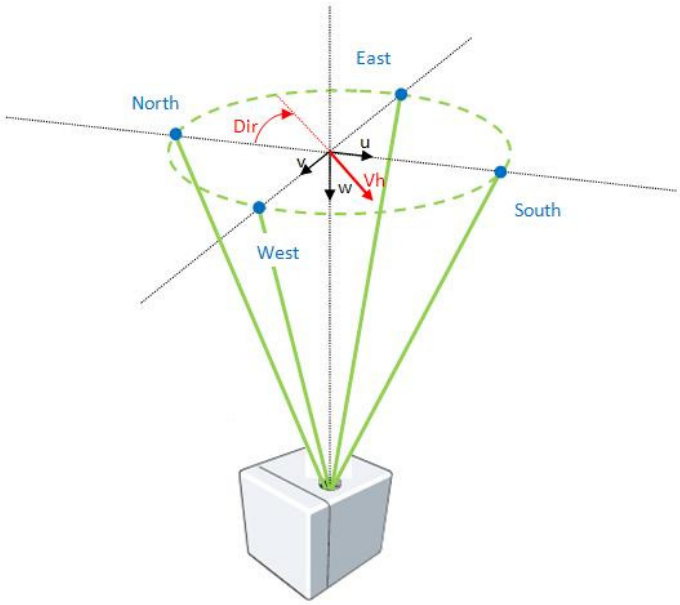

Figure 7 Orthogonal frame of the WINDCUBE for retrieving the wind speed components

Suppose the lidar probes the atmosphere with three beams in the three directions North, East, and Zenith. Then the three measured LOS velocities Vr_i are described as following (θ being the angle between Zenith and North and East, the so-called cone-angle):

$$\begin{cases} Vr_N = u\,sin\theta + w\,cos\theta \\ Vr_E = v\,sin\theta + w\,cos\theta \\ Vr_Z = w \end{cases}$$

From these equations, u, v, w can be retrieved:

$$\begin{cases} u = \dfrac{Vr_N - Vr_Z cos\theta}{sin\theta} \\ v = \dfrac{Vr_E - Vr_Z cos\theta}{sin\theta} \\ w = Vr_Z \end{cases}$$

Supposing the lidar probes the atmosphere at four different locations, the LOS being East, West, North, South, the system of wind equations will be:

$$\begin{cases} Vr_N = u\,sin\theta + w\,cos\theta \\ Vr_E = v\,sin\theta + w\,cos\theta \\ Vr_S = -u\,sin\theta + w\,cos\theta \\ Vr_W = -v\,sin\theta + w\,cos\theta \end{cases}$$

And the retrieved wind speed components, assuming they are the same at all four locations:

$$\begin{cases} u = \dfrac{Vr_N - Vr_S}{2sin\theta} \\ v = \dfrac{Vr_E - Vr_W}{2sin\theta} \\ w = \dfrac{Vr_N + Vr_E + Vr_S + Vr_W}{4cos\theta} \end{cases}$$

Horizontal wind speed V_h and wind direction Dir are then retrieved as following:

$$\begin{cases} V_h = \sqrt{u^2 + v^2} \\ Dir = Modulo(360 + atan2(v,u), 360) \end{cases}$$

If the North beam of the lidar is offset from the geographical North with an angle α, the wind direction is:

$$Dir = Modulo(360 + \alpha + atan2(v,u), 360)$$

With three beams, the solution is unique. The vertical component w is perfectly determined if the one of the three axis is accurately vertical. No check of assumptions mentioned above is possible. With four beams, the additional equation allows wind homogeneity to be checked and skip undesired values.

Cone-angle θ is a trade-off between lidar velocity resolution and atmosphere homogeneity. The smaller is θ, the better is the wind homogeneity but worse is the projection of the wind vector on every beam. M. Boquet demonstrated that best θ values are between 15° and 30°. Even in complex terrains, in general wind non homogeneity condition, no better estimation is obtained when reducing the cone angle ([18]).

2.8. Fiber lidars

Before early 2000s, LIDAR systems were based on solid-state laser technologies that do not meet operational requirements for remote site wind assessment due to high power consumption, size, weight, reliability, and life cycle cost. It was therefore the purpose of Leosphere, thanks to a partnership with French Aerospace Lab ONERA to introduce a unique fiber laser technology geared for the wind industry requirements, enabling efficient realization of compact wind Doppler lidar systems.

Fiber lidars use fiber amplifiers and coherent detection and fiber architecture based on mainstream telecommunication components. Fiber amplifiers use codoped Erbium Ytterbium silica fibers to amplify with a large bandwidth low power pulses cut out of a CW laser at 1.5µm (MOPA configuration). The electrical to optical efficiency of 1.5-µm fiber laser sources is of the order of 10%, thus allowing low electrical consumption.

This wavelength is also the most favorable for eye-safe lidar designs: the eye-safety laser energy limitation being high, the laser power can be increased with little constraints on the lidar operation or design.

One advantage of the IR fiber technology is its reliability. It is now well established that a fiber architecture is easy to adjust and mechanically reliable in a vibrating environment. The other advantages of fiber architectures are their compactness and flexibility in terms of installation. The lidar can be split up into subsystems spatially far apart and linked together using fiber optics. The new technologies of large-mode-area (LMA) fibers enable high peak power generation without nonlinear effects, while maintaining a good spatial mode and polarization state. The average power exceeds several watts and high PRF compensates efficiently the relative low pulse energy. Moreover, the MOPA architecture flexibility in terms of pulse duration allows fulfilling a large panel of requirements, either with high spatial resolution or long range.

3. Lidar performances

3.1. Noise

In coherent detection, noise sources come principally from three origins:

- LO shot noise $\langle i^2_{SN} \rangle = 2eSP_{LO}B$
- Detector noise $\langle i^2_{NEP} \rangle = 2eS\ NEP\ B$
- RIN noise $\langle i^2_{RIN} \rangle = (SP_{LO})^2 10^{RIN/10} B$

With:

- NEP: the Noise Equivalent Power density (W)
- B: the detection bandwidth

And:

$$\langle i^2_n \rangle = \langle i^2_{SN} \rangle + \langle i^2_{NEP} \rangle + \langle i^2_{RIN} \rangle$$

For optimum detection, LO shot noise must be the main noise contributor. When other sources are negligible, CNR (Carrier to Noise Ratio), describing the signal to noise ratio on the carrier frequency is:

$$CNR = \frac{\langle i^2_{het} \rangle}{\langle i^2_n \rangle} = \eta_{het} T_{inst}\ T_{atm} \cdot \frac{S}{2eB}\ \beta_\pi(Z) P_{peak}\ \tau c\ \mathrm{I}(Z)$$

3.2. Best Focus

Focus distance can be adjusted in order to optimize CNR over the measurement range. Figure 8 shows the simulated CNR variation versus focus distance, expressed as the wave radius of curvature at the instrument exit (beam radius being 11mm@1/e² at the lens).

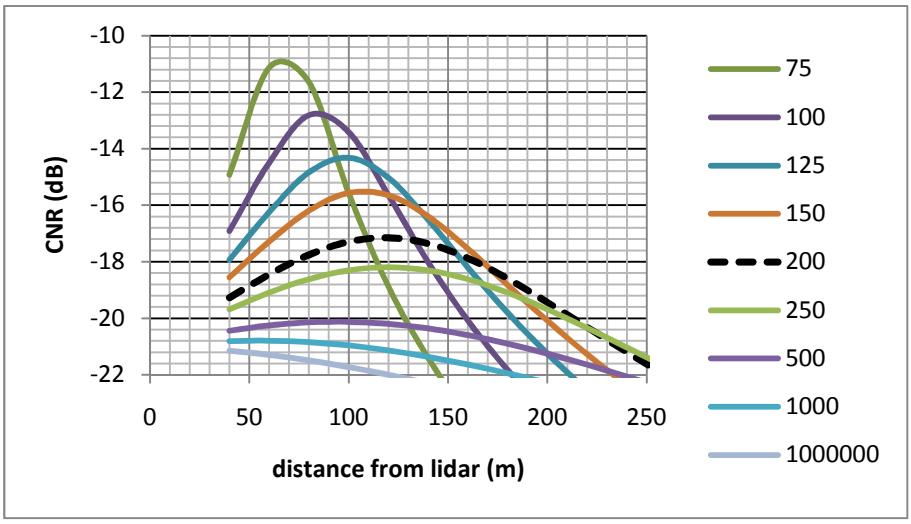

Figure 8 Variation of CNR vs distance (Altitude/cos(teta-dev)) for different beam radius of curvature

.

Best focus corresponds to maximizing the data availability at all altitudes, from H=40m (Z=46m) to H=200m (Z=230m). Practically, it corresponds to balancing and maximizing the CNR for H=40m and H=200m. For the WINDCUBE™ 7, F_{opt}=120m (H_{opt}=104m), corresponding to a beam curvature of 200m at lens (black dot line).

For a beam radius of curvature of 200m, the beam diameter slowly varies along the propagation in the range of interest. Beam radius ($1/e^2$) is σ=11mm at lens, 9mm at 46m, 7mm at 120m and 10mm at 230m, giving a maximum of 2dB difference along the total range. (CNR is proportional to $1/\sigma^2$).

Maximum focus distance corresponds to half of the Rayleigh distance Z_{ray}:

$$Z_{max} = \frac{Z_{ray}}{2} = \frac{\pi\sigma^2}{2\lambda}$$

Z_{max}=123m for the WINDCUBE™ 7 v2 parameters. This configuration minimizes the beam diameter variation from Z=0 to Z= Z_{ray} (see Figure 9).

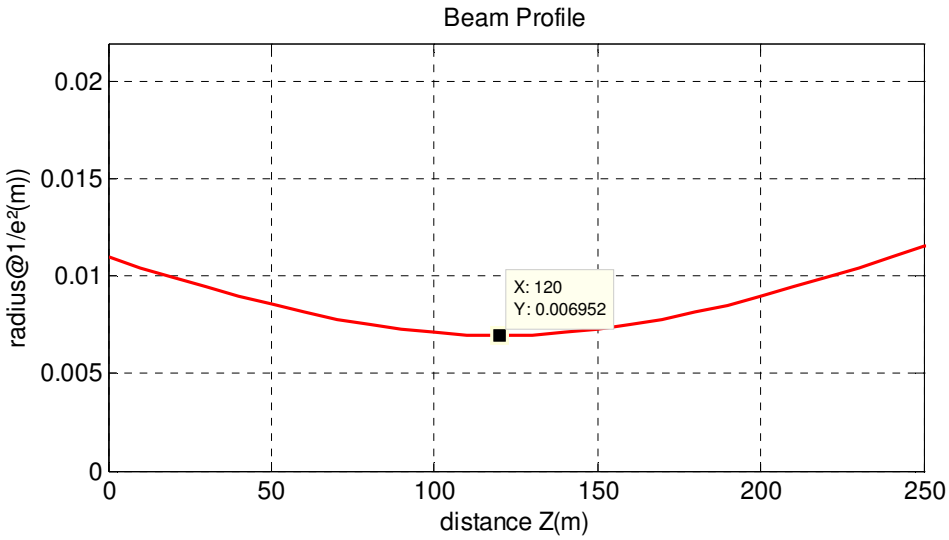

Figure 9 Beam profile along the path. Focus distance=Z_ray/2

Lindelöw, in his thesis ([14]) demonstrated a velocity error coming from the unbalanced velocity weighting function due to a variation of CNR within the range gate. In the case of the WINDCUBE™ 7 v2, the difference of CNR is always less than 0.5dB/range gate, leading to a maximum bias in the velocity of around 0.06m/s under a vertical linear wind shear of 0.02(m/s)/m (see Figure 10).

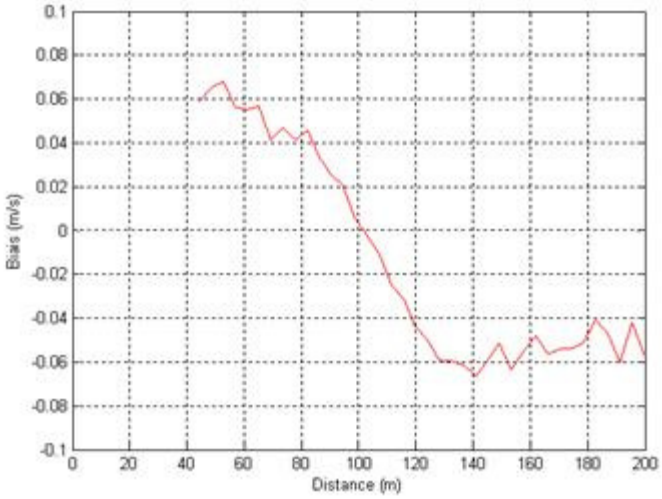

Figure 10 Simulation of the velocity bias due to the variation of CNR. Wind shear is linear and equal to 0.02(m/s)/m.

3.3. Distance range and resolution

Because of the footprint of the laser pulse on the line of sight, range resolution is limited. Moreover, during the measurement time τ_m, the pulse has moved further, enlarging the range resolution. Figure 11 describes the pulse space and time propagation and the portion of atmosphere illuminated during a time window analysis of length τ_m.

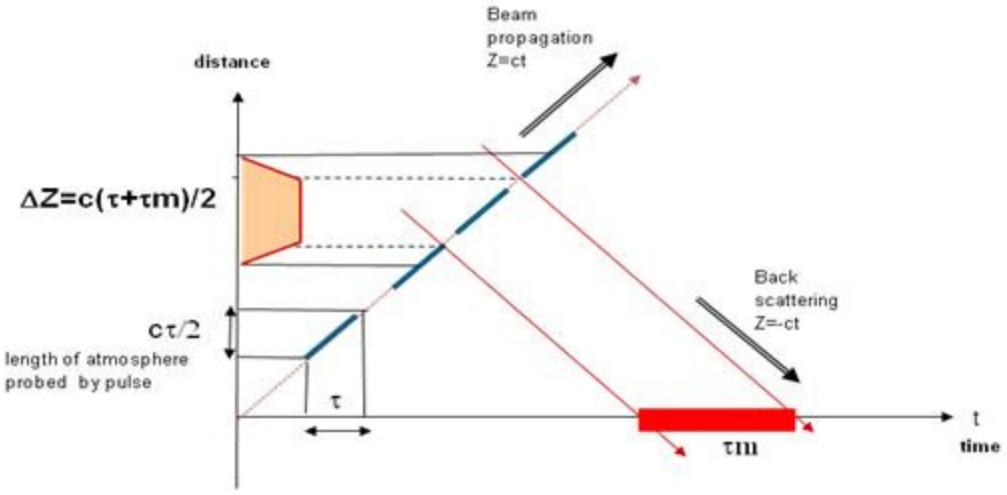

Figure 11 Pulse propagation and width of range gate represented on a time-distance plot

Velocity measurement at one point $V_d(Z)$ depends on the velocity $V_r(R)$ at close points and on the Range Weighting Function RWF(R):

$$Vd(Z) = \int_{-\infty}^{\infty} RWF(R)Vr(R)dR$$

For a pulsed lidar, Banakh and Smalikho give an analytical equation of the range gate weighting function RWF ([7]), when the pulse is Gaussian (FWHM=τ) and range gate is flat (width τ_m), as the convolution between the pulse power profile and the range gate profile:

$$RWF(Z) = \frac{1}{\tau_m c}\left[\operatorname{erf}\left(\frac{4\sqrt{\ln(2)}}{c\tau}(Z - Z_0) + \frac{\sqrt{\ln(2)}\,\tau_m}{\tau}\right) - \operatorname{erf}\left(\frac{4\sqrt{\ln(2)}}{c\tau}(Z - Z_0) - \frac{\sqrt{\ln(2)}\,\tau_m}{\tau}\right)\right]$$

Range resolution is defined as the FWHM of the function RWF which is roughly:

$$\Delta z1 = \frac{c\tau_m}{2\ \operatorname{erf}\left(\sqrt{\ln(2)}\,\frac{\tau_m}{\tau}\right)}$$

Banakh and Smalikho noted that, for the same parameters, the resolution estimated with their method is about one and a half lower than the estimate done by Frehlich ([8]). Frehlich simply summed the FWHM of the pulse and the length of measurement window.

Considering a Gaussian pulse shape (FWHM=165ns) and flat range gate (265ns), RWF can be estimated according to Banakh and Smalikho (Figure 12). The calculation of range resolution approximation gives a resolution of about 40m.

This method leads to the same results as a simple convolution of the Pulse and the Range Gate (39m, see Figure 13).

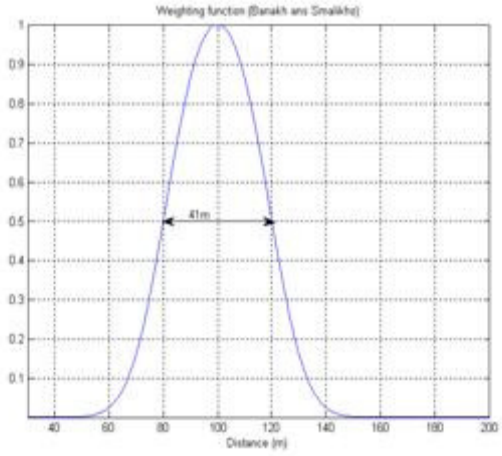

Figure 12 RWF according to Banakh And Smalikho

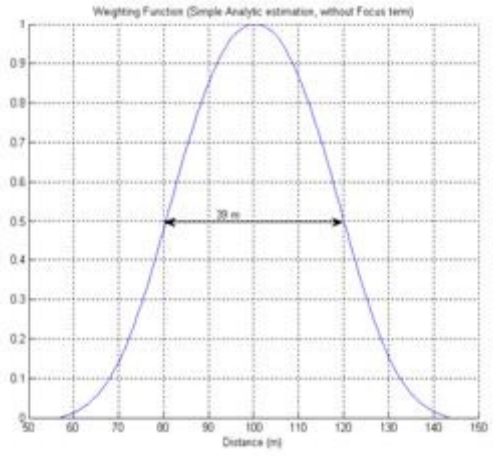

Figure 13 Convolution of Pulse Shape and Range Gate

This simulation is adapted for collimated system but does not give accurate results for focused lidars, i.e. focusing the laser beam leads to better resolution near the focusing point. Moreover, this method is only valid for a Gaussian Pulse and a flat measurement window.

In order to make this calculation more general, Lindelöw ([14]) proposed multiplying the focusing efficiency by the convolution of the pulse and the range gate profile.

$$RWF(Z) = \eta_{foc}(Z).(Pulse * FFT_{window})(Z)$$

With $\eta_{foc}(Z)$ the focusing efficiency:

$$\eta_{foc}(Z) = \left(1 + Z_r^2\left(\frac{1}{Z} - \frac{1}{Z_{foc}}\right)\right)^{-1},$$

Range Weighting Function is estimated according to this method (Figure 14). FWHM is found to be 33.6m.

An efficient method to theoretically evaluate the range resolution is to calculate the lidar response to the propagation of a pulse through a wind speed "Dirac", this is the "Impulse Response". On Figure 15 is represented a brutal change of wind speed value at 100m distance from the pulsed lidar (black dots) and the lidar velocity estimation from 40m to 200m (red curve) with Gaussian pulse and flat range gate. The distance, at which the wind speed retrieval process is not influenced anymore by the "Dirac", indicates the distance resolution. Here the "Impulse Response" FWHM appears to be 34.8m.

Good agreement between Lindelöw method and the "Impulse Response" is obtained.

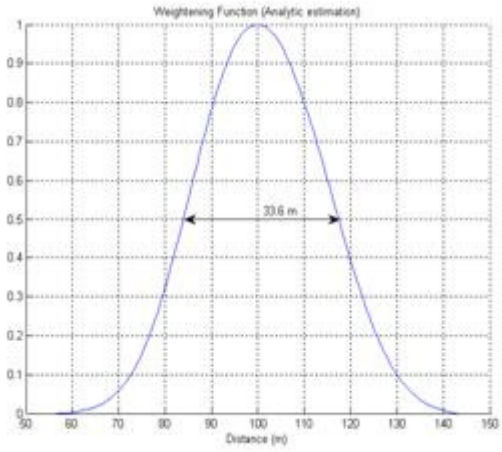

Figure 14 RWF according to Lindelöw method

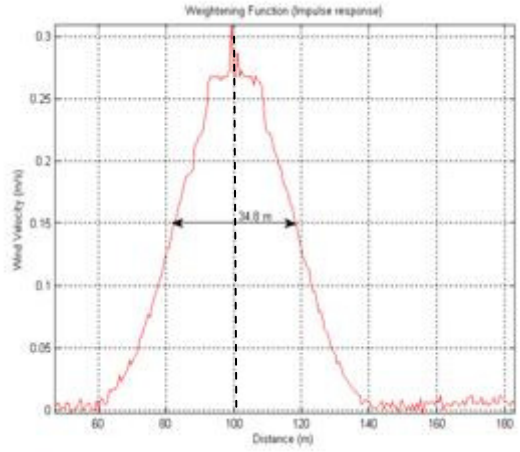

Figure 15 "Dirac" wind speed (black dots) and simulated "Impulse Response" (red)

These methods can also be applied to the current WINDCUBE™ 7 v2 pulse shape (Figure 16) and range gate profile (Figure 17).

On Figure 18 the "Impulse Response" is represented. FWHM is calculated to be 27m. The altitude resolution is therefore around 23.8m (LOS zenithal deviation angle is 28°).

Lindelöw RWF estimation is given on Figure 19 and distance resolution is 26.3m, i.e. ~23.2m altitude resolution.

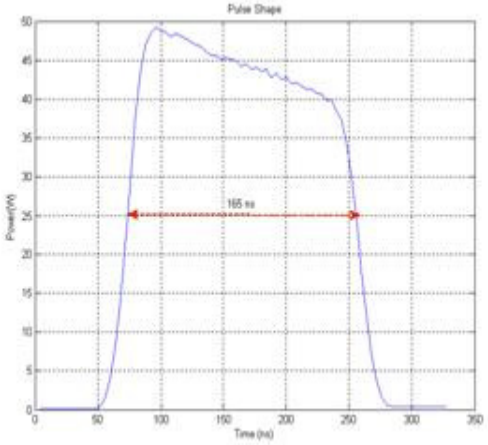

Figure 16 Pulse Shape for WINDCUBE™ 7 V2

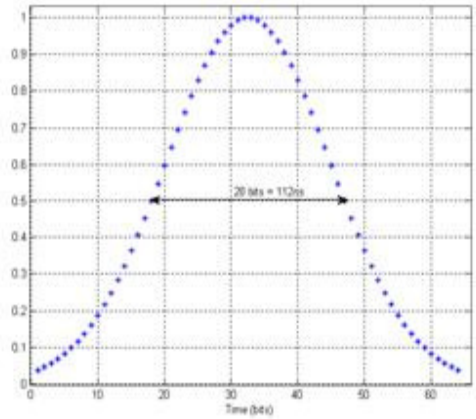

Figure 17 Range Gate Window for WINDCUBE™ 7 V2

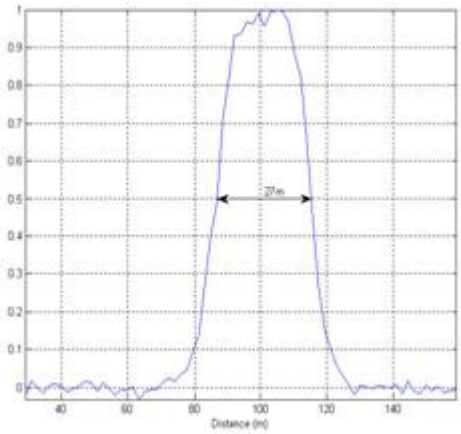

Figure 18 "Impulse Response" for WINDCUBE™ 7 V2

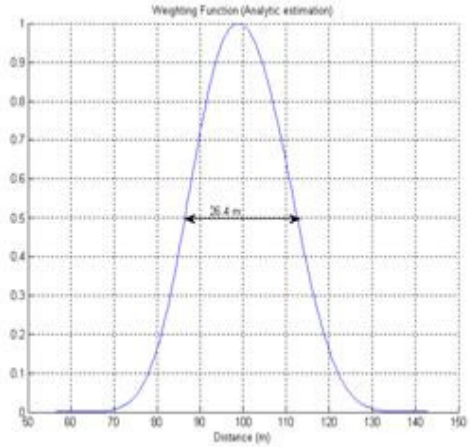

Figure 19 RWF according to Lindelöw method for WINDCUBE™ 7 V2

3.4. Velocity range and resolution

3.4.1. Velocity range and ambiguity

Radial velocity is proportional to Doppler frequency shift. Velocity range is then determined by frequency range. The intermediate frequency F_i used in most pulsed lidars permits the measurement of both positive and negative shifts. Maximum downshift is limited by the value of F_i, since no negative frequency can be measured. Maximum upshift is limited by the Nyquist frequency, half of the sampling frequency F_s. Figure 20 describes the spectrum and velocity ranges.

Because of spectral extent of the signal and low frequency noise, this range is in fact a bit smaller. For example, with λ=1.55µm, F_i =68MHz and F_s =250MHz, the practical horizontal velocity range is [-50m/s, +50m/s].

A pass-band filter cancels outband Doppler shifts to avoid Doppler ambiguities.

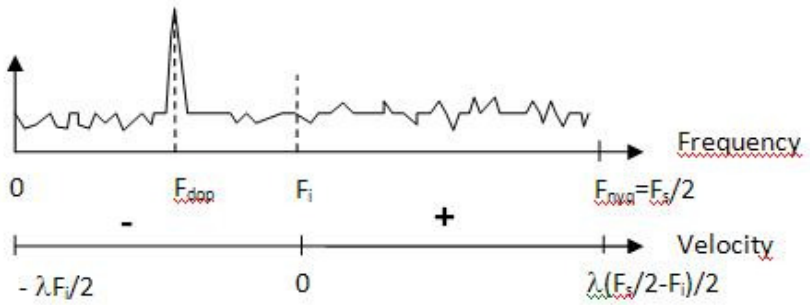

Figure 20 Lidar spectrum and velocity range

3.4.2. Velocity resolution

Velocity precision depends on both atmospheric parameters and lidar parameters. Both are broadening the Doppler spectrum and hence limit the frequency estimation. Atmospheric parameters are wind gradient within the range gate and turbulence. Lidar parameters are pulse duration CNR and number N of averaged spectra. The smaller the pulse duration, the smaller the range gate and the velocity dispersion but larger the frequency spectrum.

The equation below gives the minimum velocity resolution as a function of relative parameters. It is called Cramer-Rao Lower Bound (CRLB).

$$\sigma_{Vcrlb} = \sqrt{2}\frac{\lambda}{2\tau}\frac{\sqrt{1+CNR}}{\sqrt{N}CNR}$$

This equation assumes an infinite correlation time of the signal. In an actual lidar, σ_v is limited by the finite correlation time τ_c, the smallest value between the pulse duration and the correlation time of the atmosphere.

$$\sigma_{Vsat} = \frac{\lambda}{2}\frac{1}{\sqrt{N}}\frac{1}{4\pi\tau_c}$$

The global velocity resolution is then:

$$\sigma_V = \sqrt{{\sigma_{Vcrlb}}^2 + {\sigma_{Vsat}}^2}$$

Figure 21 illustrates the variation of σ_v with CNR for N=100 and N=10000. For low CNR values, σ_v decreases as 1/CNR. Doubling the pulse energy divides by 2 the velocity resolution. For high CNR values, σ_v is constant. Spectral broadening comes from speckle fluctuations in the signal. The only way to reduce σ_v is to increase N. For intermediate CNR, σ_v varies as $1/\sqrt{CNR}$. It is therefore equivalent to increase pulse energy or number of pulses. In this region, σ_v depends only on the average laser power. Using a low energy, high pulse repetition rate (PRF) laser is then equivalent to using a high energy, low PRF laser, assuming the average power is constant. This is one for the reasons of the recent emergence of high PRF fiber lasers for pulsed Doppler lidars.

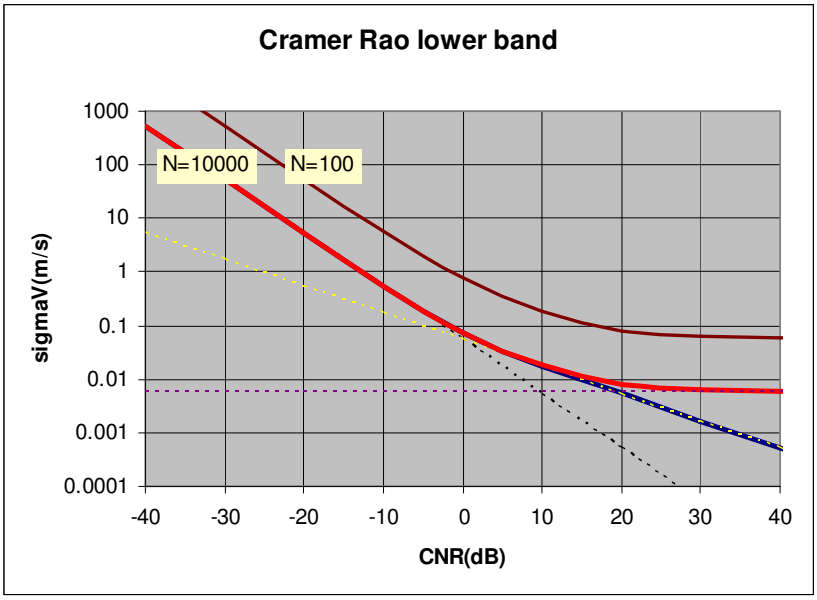

Figure 21 Cramer Rao Boundary for 100 averaged spectra (dark red) and 10000 averaged spectra (light red). CNR is measured in narrow band (B=1/τm)

3.4.3. Range ambiguity

The rate at which pulses are transmitted, the Pulse Repetition Frequency (PRF) limits the range over which heights can be unambiguously determined. To avoid ambiguity between return signals, the Inter Pulse Period (IPP=1/PRF) must be longer than the round trip time of flight of the pulse to the greatest height.

$$PRF_{max} = \frac{C}{2Z_{max}}$$

For example, to measure without ambiguity up to 5km, the PRF needs to be less than 30KHz.

3.4.4. Time-Bandwidth Tradeoffs

Spatial resolution is proportional to pulse duration. The shorter the pulse, the smaller the resolution. Velocity resolution is proportional to spectrum width and is smaller when the spectrum is narrow. Because the spectrum width is inversely proportional to the pulse duration, range resolution and velocity resolution are also inversely proportional.

3.5. Instrumental uncertainties

From the emission of laser light to the retrieval of the wind speed there are a defined number of hardware, software and atmospheric parameters which might introduce biases and uncertainties in the final result. If the atmospheric uncertainties are difficult to assess, it is possible to analyze the influence of variations in the hardware components and their impact on the measurement. This chapter aims to assess the instrumental uncertainties and what can be the statistical errors and biases.

Horizontal velocity V_h is given by:

$$V_h = \sqrt{u^2 + v^2}$$

$$u = \frac{Vr_N - Vr_S}{2sin\theta} \qquad v = \frac{Vr_E - Vr_W}{2sin\theta}$$

$$Vr_i = \frac{\lambda}{2}(fd_i - f_{AOM}) \quad with\ i = N, S, E, W$$

With:

- fd_i : the Doppler frequency shift that is estimated
- f_{AOM} : the AOM frequency

$$u = \lambda\frac{fd_N - fd_S}{4sin\theta} \qquad v = \lambda\frac{fd_E - fd_W}{4sin\theta}$$

Thus, u and v do not depend on f_{AOM}.

Studying V_h variations:

$$\Delta V_h = \frac{u\Delta u + v\Delta v}{\sqrt{u^2 + v^2}} = cos\varphi\Delta u + sin\varphi\Delta v$$

With φ: wind azimuth angle

$$\Delta u = u\frac{\Delta\lambda}{\lambda} + u\frac{\Delta\theta}{tan\theta} + \lambda\frac{\Delta fd}{2sin\theta}$$

Since

$$\Delta u < V_h\left(\frac{\Delta\lambda}{\lambda}+\frac{\Delta\theta}{tan\theta}\right)+ \lambda\frac{\Delta fd}{2sin\theta}$$

And

$$\Delta v < V_h\left(\frac{\Delta\lambda}{\lambda}+\frac{\Delta\theta}{tan\theta}\right)+ \lambda\frac{\Delta fd}{2sin\theta}$$

$$cos\varphi + sin\varphi < \sqrt{2}$$

We finally have:

$$\Delta V_h < \sqrt{2}\left[V_h\left(\frac{\Delta\lambda}{\lambda}+\frac{\Delta\theta}{tan\theta}\right)+ \lambda\frac{\Delta fd}{2sin\theta}\right]$$

Because the laser is developed for WDM (wavelength multiplexing) telecom applications, master oscillator wavelength is known with a good accuracy, i.e. <0.1nm (10GHz).

$$\text{So } \frac{\Delta\lambda}{\lambda} < 10^{-4}$$

Uncertainty on angle comes from mechanical manufacturing of the telescopes. Angles are measured on all axes of all optical heads and are validated when $\theta = 28° \mp 0.08°$.

$$\text{So } \frac{\Delta\theta}{tan\theta} < 2.6\ 10^{-3}$$

Uncertainty on Doppler frequency f_d comes from an uncertainty on sampling frequency f_{ech} and from estimation of the line centroid x_i in the spectrum vector.

$$fd_i = fech.\frac{x_i}{Nfft}$$

$$\Delta fd_i =.\frac{f_{ech}}{Nfft}\Delta x + \frac{x_i}{Nfft}\Delta f_{ech}$$

x_i is the exact position of the frequency line in the spectrum vector, given by the Doppler shift frequency estimator MLE. N_{fft} is perfectly known. Δ_x comes from MLE processing and is not considered in this chapter.

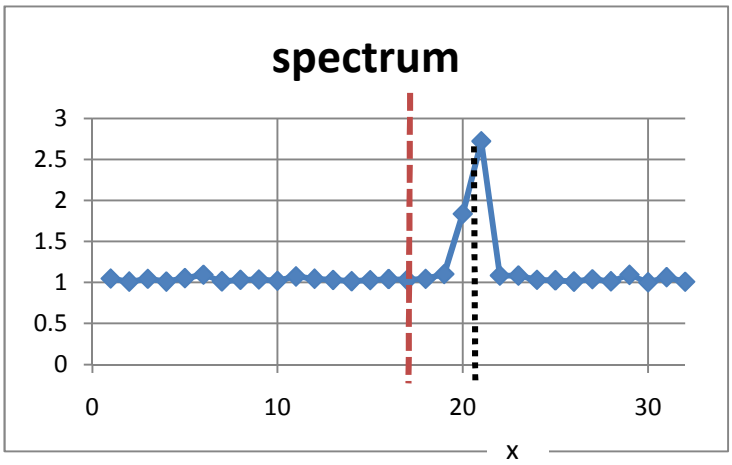

Figure 22 Spectrum power vs frequency bins - Nfft=64, Vh=10m/s, fmao=68MHz

$$x_i < \frac{Nfft}{2} \qquad \Delta fd_i < \frac{\Delta f_{ech}}{2}$$

f_{ech} is given by an accurate quartz crystal on the acquisition board. The accuracy, given by the manufacturer is 2ppm. So $\Delta f_{ech} < 2\ 10^{-6} f_{ech}$ and $\Delta fd_i < 250Hz$.

$$\Delta V_h < \sqrt{2}\left[V_h \left(\frac{\Delta\lambda}{\lambda} + \frac{\Delta\theta}{tan\theta}\right) + \lambda \frac{\Delta fd}{2sin\theta}\right]$$

$$\Delta V_h < \sqrt{2}[\, V_h(10^{-4} + 2.6\ 10^{-3}\,) + 4\ 10^{-4}]$$

$$\Delta V_h < 3.8\ 10^{-3}\, V_h + \ 5.6\ 10^{-4}$$

Since the second term is negligible, the relative uncertainty on V_h is about 0.38%. The major contributor (96%) is the uncertainty on the zenithal angle.

In conclusion, the relative uncertainty on the horizontal wind speed, according to the uncertainty study of internal parameters (wavelength, sampling frequency, zenithal angle) is small (< 0.04m/s for V_h=10m/s) and negligible when compared to the frequency estimation by the MLE and atmospheric origins (turbulence, shears).

3.6. Existing systems and actual performances

In 2010, only a few pulsed lidars are available. Table 4 summarizes the characteristics of commercial ones, which can be used in the wind industry, meteorology or airport safety.

System	Wave-length (µm)	Range (m)	Accuracy (m/s)	Data update	Sample volume length (m)	Pulse duration	Pulse energy	PRF	Beams configuration
Leosphere WINDCUBE™7	1,5	40-200	0.1	1s/10alt	20	200ns	10µJ	20KHz	Four beams
LMCT WindTracer	2	500-5000	1	0.1s	60	400ns	2mJ	500 Hz	LOS mapping
Mitsubishi Electrics	1,5	100-1500	N.A	1s	90	600ns	6.5µJ	1KHz	Scanning head
Halophotonics Gallion	1,5	30-2000	0,25	0,1-30s	20-60	150 ns	10µJ	20KHz	LOS mapping
CatchTheWind Vindicator	1,5	NA	NA	NA	NA	NA	NA	NA	three telescopes

Table 4 Comparison of commercially available pulsed lidars.

3.7. Verification and validation of performances

Since the instrumental sources of uncertainty are now well identified and the range of deviation they might incur in the wind speed measurement are well estimated, it is necessary to compare the measurement of a new lidar unit against a tall mast equipped with traditional anemometry or against a well-known and validated lidar in a double phase verification/validation.

Verification is the quality control process of evaluating if a new WINDCUBE™ is acting in conformity with the specified standard performances expected for every WINDCUBE™ unit. During this process, every source of bias and uncertainty identified is checked to ascertain whether its performance is within the specified range. The parameters checked include the laser output power, the laser pulse shape, and the laser beam focusing distance. Their performances are checked in a series of qualification tests including shocks and vibration and temperature variations.

Validation is the process of ensuing that a WINDCUBE™ measures wind speed characteristics in conformity with what a reference instrument would give. Today, validation is done against well-known traditional anemometry, like a mast equipped with calibrated cup anemometers. This instrument comparison introduces additional uncertainties, not related to the inner performances of each individual instrument but related to the differences in the measurement process between the two instruments ([23]). These differences in the measurement process might incur differences in measured values, which will be site and time specific. Even if these are small, it is important to closely define the range of variation that might occur on the validation site.

LEOSPHERE has developed a unique qualification process for verification and validation of every new WINDCUBE™ unit, which consists of a verification phase as described above and a WINDCUBE™ units' comparison phase. The retrieved parameters of a new unit are compared to retrieved parameters of reference units which performances are themselves validated by external wind experts. Compared variables at different heights are among others CNR, horizontal wind speed, dispersion of horizontal wind speed, wind direction, vertical wind speed and data availability. After a validation period, an acceptance metrics is filled and the parameters are compared to tolerance thresholds for acceptance or rejection of the unit. The resulting scores are stored and account for the unit quality control ID. This process leads to an estimation of the instrument uncertainty as a combination of the reference unit uncertainty evaluated by external wind experts and the resulting WINDCUBE™s inter-comparison uncertainty.

Following such a manufacturing process with strict rules and protocols ensures a very good unit to unit repeatability, proven by the large number of WINDCUBE™ units send to and validated by external wind experts.

4. Conclusions and Perspectives

This report summarizes the principles of operation, the performances and critical parameters of Doppler pulsed wind lidars, such as the WINDCUBE™ lidar from LEOSPHERE. It takes into account the different steps of the velocity measurement process to ensure a strict control of the lidar from development and optimization to serial production.

More generally, pulsed and continuous wave lidars have shown great reliability and accuracy in the measurement of wind characteristics such as horizontal and vertical wind speed and wind direction at various heights on flat terrains and offshore ([17], [21]). The high data recovery rate up to above blade top ensures a high quality analysis of the wind conditions available on the project site, leading to an optimized layout design and the choice of the suitable turbines.

Regarding future improvements, the measurement of additional wind parameters like turbulence intensities, kinetic fluxes or inflow-angles is under investigation at the present time and should be available in the near future.

One of the other remaining challenges is also reaching high accuracy in complex terrains where flow distortion occurs and impairs the lidar wind components retrieval from measured radial velocities. Since lidar radial velocities are still very accurate even on complex and rough terrains, a methodology using CFD modeling has been recently developed to avoid taking the flow homogeneity assumption ([19], [20]). Even though new, this methodology has already shown good results on sites of various complexities, and is currently being furthermore studied.

To sum up, lidar anemometry has already proven its great utility in the development of wind farm projects, as an instrument allowing considerable financial gains through a better understanding of the wind conditions at a site and therefore reducing the capital risk of the investors ([24]), but also for operational power curves measurements ([22]). With the general trend to develop larger wind turbines and wider wind farms, the lidar technology is elected to be more and more widely used.

5. References

[1] M. J. Levin, “Power Spectrum Parameter Estimation”, IEEE Transactions on Information Theory Vol. IT-11 pp. 100-107, 1965.

[2] A.E. Siegman, “The antenna properties of optical heterodyne receivers”, Appl. Opt. 5, pp. 1588-1594, 1966.

[3] Rod G. Frehlich and Michael J. Kavaya, “Coherent laser radar performance for general atmospheric refractive turbulence”, APPLIED OPTICS, vol. 30, no. 36, 1991.

[4] Richard Bamler, “Doppler Frequency Estimation and the Cramér-Rao Bound”, IEEE Transactions on Geoscience and Remote Sensing Vol. 29 No. 3 pp. 385-390, 1991.

[5] Rod G. Frehlich, “Cramér-Rao Bound for Gaussian Random Processes and Applications to Radar Processing of Atmospheric Signals”, IEEE Transactions on Geoscience and Remote Sensing Vol.31 No.6 pp. 1123-1131, 1993.

[6] Barry J. Rye, R. Michael Hardesty, “Discrete Spectral Peak Estimation in Incoherent Backscatter Heterodyne Lidar. I: Spectral Accumulation and the Cramér-Rao Lower Bound”, IEEE Transactions on Geoscience and Remote Sensing Vol. 31 No. 1 pp. 16-27, 1993.

[7] V. Banakh, I. Smalikho, “Estimation of the turbulence energy dissipation rate from the pulsed Doppler lidar data”, J. Atmos. Oceanic. Opt., vol. 10, n°12, December 1994.

[8] Rod G. Frehlich, Stephen M. Hannon and Sammy W. Henderson, “Performance of a 2- Coherent Doppler Lidar for Wind Measurements”, J. Atmos. Oceanic Technol., vol. 11, no. 6, p. 1517, December 1994.

[9] Philippe Salamitou, Alain Dabas, Pierre H. Flamant, “Simulation in the Time Domain for Heterodyne Coherent Laser Radar”, Applied Optics Vol. 34 No. 3 pp. 499-506, 1995.

[10] R.M. Huffaker and R. Michael Hardesty, “Remote Sensing of Atmospheric Wind Velocities Using Solid-State and CO2 Coherent Laser Systems”, Proceedings IEEE, vol. 84, no. 2, p. 181 February 1996.

[11] D. Soreide, Rodney K. Bogue, Jonathan Seidel and L. J. Ehernberger, “The Use of a Lidar Forward-Looking Turbulence Sensor for Mixed-Compression Inlet Unstart Avoidance and Gross Weight Reduction on a High Speed Civil Transport”, NASA Technical Memorandum 104332, July 1997.

[12] Rod G. Frehlich, Stephen M. Hannon and Sammy W. Henderson, “Coherent Doppler Lidar Measurements of Wind Field Statistics”, Boundary-Layer Meteorol. 86, pp. 233–256, 1998.

[13] J.P. Cariou, B. Augere and M. Valla, “Laser source requirements for coherent lidars based on fiber technology”, Comptes Rendus Physique, Volume 7, Issue 2, Pages 213-223, High power fiber lasers, and amplifiers, March 2006.

[14] P. Lindelöw, “Effective sample volume Fiber Based Coherent Lidars for Remote Sensing of Wind”, Thesis from Technical University of Denmark, p 63-76, 2008.

[15] T. Ando, S. Kameyama, Y. Hirano, “All-fiber Coherent Doppler LIDAR technologies at Mitsubishi Electric Corporation”, 14th International Symposium for the Advancement of Boundary Layer Remote Sensing IOP Conf. Series: Earth and Environmental Science 1 012011, 2008.

[16] T. Mikkelsen, “WINDSCANNER: -a Facility for Wind and Turbulence Measurements around large Wind Turbines”, In Nordic Conf. on: Global Challenges -Regional Opportunities: How can Research Infrastructure and eScience support Nordic competitiveness? Topic: Climate, Energy and Environment, Stockholm 12-13 Nov. 2008.

[17] M.S. Courtney, R. Wagner and P. Lindelöw, “Commercial Lidar Profilers for Wind Energy. A comparative Guide”, EWEC 2009.

[18] M. Boquet, R. Parmentier, J.P. Cariou, “Analysis and Optimization of Pulsed Doppler Lidar in Complex Terrain”, EWEC 2009.

[19]F. Bingol, J. Mann, D. Foussekis, “Conically Scanning Lidar Error in Complex Terrain”, Meteorologische Zeitschrift, Vol. 18, No. 2, 001-007, April 2009.
[20]M. Boquet, R. Parmentier, J.P. Cariou, “Correction of Pulsed Wind Lidar Bias in Complex Terrain”, ISARS 2010.
[21]A. Westerhellweg, A. Beeken, B. Canadillas, T. Neumann, “One Year of Lidar Measurements at FINO1-Platform: Comparison and Verification to Met-Mast Data”, DEWEK 2010.
[22]J. Gottschall, M.S. Courtney, P. Lindelöw, A. Albers, “Classification of Lidar Profilers or: How to Introduce Lidars to Power Performance Testing”, Proceedings EWEC 2010.
[23]A. Albers, A.W. Janssen, J. Mander, “How to Gain Acceptance for Lidar Measurements”, DEWEK 2010.
[24]M. Boquet, P. Callard, N.Deve and E.G. Osler, “Return on Investment of a Lidar Remote Sensing Device”, DEWI Magazin No. 37, pp. 56-61, August 2010.